catalysts

MDPI

*Article*

# Enhancing Electron Transfer in Cytochrome P450 Systems: Insights from CYP119–Putidaredoxin Interface Engineering

**Akbota Kakimova [1] and Nur Basak Surmeli [2,*]**

[1] Department of Biotechnology and Bioengineering, Izmir Institute of Technology, Gülbahce, Urla 35430, İzmir, Turkey
[2] Department of Bioengineering, Izmir Institute of Technology, Gülbahce, Urla 35430, Izmir, Turkey
* Correspondence: nursurmeli@iyte.edu.tr; Tel.: +90-232-750-6955

**Abstract**

Cytochrome P450 enzymes (CYPs) are versatile biocatalysts capable of performing selective oxidation reactions valuable for industrial and pharmaceutical applications. However, their catalytic efficiency is often constrained by dependence on costly electron donors, the requirement for redox partners, and uncoupling reactions that divert reducing power toward reactive oxygen species. Improving electron transfer efficiency through optimized redox partner interactions is therefore critical for developing effective CYP-based biocatalysts. In this study, we investigated the interaction between CYP119, a thermophilic CYP from *Sulfolobus acidocaldarius*, and putidaredoxin (Pdx), the redox partner of P450cam. Using rational design and computational modeling with PyRosetta 3, 14 CYP119 variants were modeled and analyzed by docking simulations on the Rosie Docking Server. Structural analysis identified three key mutations (N34E, D77R, and N34E/D77R) for site-directed mutagenesis. These mutations (N34E, D77R, and N34E/D77R) enhanced Pdx binding affinity by 20-, 3-, and 12-fold, respectively, without affecting substrate binding. Catalytic assays using lauric acid and indirect assays to monitor electron transfer revealed that, despite improved complex formation, the N34E variant showed reduced electron transfer efficiency compared to D77R. These findings highlight the delicate balance between redox partner binding affinity and catalytic turnover, emphasizing that fine-tuning electron transfer interfaces are essential for engineering efficient CYP biocatalysts.

**Keywords:** biocatalysis; enzymes; hemoproteins; protein engineering; Cytochrome P450

check for updates

Academic Editor: David D. Boehr

Received: 8 October 2025
Revised: 17 October 2025
Accepted: 20 October 2025
Published: 21 October 2025

**Citation:** Kakimova, A.; Surmeli, N.B. Enhancing Electron Transfer in Cytochrome P450 Systems: Insights from CYP119–Putidaredoxin Interface Engineering. *Catalysts* **2025**, *15*, 1000. https://doi.org/10.3390/catal15101000

**Copyright:** © 2025 by the authors. Licensee MDPI, Basel, Switzerland. This article is an open access article distributed under the terms and conditions of the Creative Commons Attribution (CC BY) license (https://creativecommons.org/licenses/by/4.0/).

## 1. Introduction

Cytochrome P450s (CYPs) are remarkably complex enzymes functioning as an external monooxygenase that utilize an external reductant in their reactions [1–3]. CYPs can efficiently regio- and stereoselectively catalyze an enormous variety of oxidative processes [4,5]. Commonly, CYPs catalyze the addition of a single oxygen atom of $O_2$ to both endogenous and exogenous substrates for a variety of oxidative processes via the traditional two-electron oxo-transfer pathway [5–7]. CYP reactions involve supporting proteins that are redox partners and consumption of reducing agents, and most CYPs use pyridine nucleotide, usually NADH or NAD(P)H, as a cofactor [8]. Redox partners are supporting proteins that affect the transfer of electrons in CYP catalytic reactions [9,10]. For example, putidaredoxin reductase (PdR), containing a flavin adenine dinucleotide (FAD), and putidaredoxin (Pdx), comprising an [2Fe–2S]-type iron–sulfur protein, are supporting proteins involved in transferring electrons from NAD(P)H electron donor to CYP101 (P450cam) enzyme [11–13].

Despite the enormous practical potential of CYPs, the redundancy of P450 redox systems can restrict the use of these enzymes in manufacturing processes [14]. The main limitations of these enzymes are: (a) the need for specific electron transfer partners; (b) the need for costly and unstable electron donors such as NAD(P)H; and (c) uncoupling during oxidation, employing NAD(P)H as an electron source without yielding a product [3,14,15]. It was reported that reactive oxygen species can arise due to possible electron leaking on the substrate binding step $Fe^{3+}O_2^-$ and $Fe^{3+}O_2^{2-}$. Furthermore, two water molecules can be formed, and four electrons can be consumed without simultaneous substrate hydroxylation. As a result, no hydroxylated product is observed, but the costly cofactor NAD(P)H has been utilized [3]. Moreover, the heme cofactor may become unstable, and the apoprotein degrades due to the generation of harmful hydrogen peroxide or active oxygen species [3]. Efficient oxygen activation and product generation depend on interactions between enzyme and redox proteins, and by optimizing electron flow, improvements in substrate conversion can be obtained [3].

CYP119 is the first identified thermophilic CYP from *Sulfolobus acidocaldarius*, and it catalyzes the hydroxylation of lauric acid utilizing the P450cam redox partners Pdx and PdR [14,16]. Early site-directed mutagenesis showed that single-surface substitutions can strongly modulate activity: T214V and D77R increase lauric acid hydroxylation by ~6- and ~13-fold, respectively, and D77R decreases the Pdx–CYP119 dissociation constant from ≈2.1 mM to ≈0.5 mM while enhancing electron-transfer rates, demonstrating that interface engineering can improve catalytic throughput in this thermophilic system [14]. Despite this significant enhancement, a substantial gap remains when comparing CYP119's binding affinity to the highly efficient, native P450cam−Pdx complex, which exhibits $K_d$ values in the micromolar range (5–17 μM) [17–19]. This disparity suggests that the current engineered CYP119−Pdx interface is still suboptimal for rapid and efficient electron transfer. Crucially, previous interface engineering efforts, including the successful D77R mutation, were performed without the benefit of high-resolution structural data for the P450cam−Pdx complex and before the widespread use of sophisticated computational docking and structural analysis tools that allow for detailed residue-level investigation of protein–protein interactions.

Recent advancements in P450 engineering have further underscored the importance of the electron transfer interface, with successful strategies falling into two main categories: the creation of highly efficient self-sufficient P450 fusion enzymes (e.g., P450BM3 chimeras) and rational interface redesign in two-component systems. The latter, which is most relevant here, has been revolutionized by high-resolution structural and computational tools, including molecular docking and dynamics (MD) simulations, allowing researchers to precisely optimize the distance and orientation of redox cofactors [7,20]. These modern studies often target shortening the electron transfer distance and improving the conformational sampling that promotes the active state of the P450 [20,21]. However, despite this progress, there remains a clear gap in the rational, structure-guided optimization of the thermophilic CYP119 system. This study was designed to apply modern computational and structural analysis techniques to the CYP119−Pdx interface, moving beyond earlier site-directed mutagenesis efforts to identify and introduce novel mutations that further improve the binding affinity and electron transfer efficiency beyond the current D77R benchmark.

In this study, we addressed the challenge of enhancing P450 catalytic efficiency through rational interface engineering of the CYP119–Pdx complex. Using PyRosetta 3 and the ROSIE Docking Server, we modeled 14 CYP119 variants and experimentally characterized three promising mutants: N34E, D77R, and the double mutant N34E/D77R. The N34E substitution produced a ~20-fold increase in Pdx binding affinity, yet catalytic assays revealed an unexpected outcome—stronger binding did not improve electron transfer

efficiency. Instead, the N34E mutant transferred electrons more slowly than D77R, despite its tighter association. This finding challenges the common assumption that enhanced redox partner affinity directly leads to higher catalytic turnover. By revealing how excessive interface stabilization can hinder productive electron transfer, our work provides new molecular insight into the rate-limiting dynamics of P450 catalysis and establishes a refined framework for engineering more efficient CYP biocatalysts for industrial and therapeutic applications.

## 2. Results

### *2.1. Design of CYP119 Mutant Enzymes and Protein–Protein Docking*

Previous studies have shown that CYP119 can accept electrons from putidaredoxin (Pdx) and putidaredoxin reductase (PdR) with low efficiency [22]. The native redox partner for Pdx and PdR is the bacterial CYP enzyme—P450cam (CYP101) [22–24]. To improve the electron transfer efficiency of the three-protein system with CYP119-Pdx-PdR, structural alignment of P450cam (PDB ID:4JWS), Pdx (PDB ID: 1XLN), and CYP119 (PDB ID: 1IO7) proteins was performed. Structural and sequence alignments of CYP119 and P450cam are shown in Figures S1 and S2.

For the mutagenesis studies, non-conserved residues on the possible binding surface of CYP119 were selected based on previous studies. According to the structural alignment results, four residues were selected for mutations: Asn34, Asn35, Lys30, and Asp77. The structural alignment results showed that Lys30, Asn34 and Asn35 corresponded to Arg72, Glu76 and Asp77 in P450cam. These three residues could potentially form important interactions with positively charged Arg66 residue of Pdx; therefore, they were chosen for mutation. Asp77 of CYP119 corresponds to Arg109 residue in P450cam. D77R mutant was selected because previous studies showed that this mutation resulted in a 5-fold enhancement in the rate of electron transfer between Pdx and CYP119 [14]. Mutated residues in CYP119, corresponding residues in P450cam, their possible interaction sites on Pdx, and modeled mutations are summarized in Table S1.

Based on the structural alignment results, six single and eight double mutants were selected for docking studies. PyRosetta 3 Software was used to design mutant proteins; the designed proteins showed similar stability to WT CYP119, as seen from the similar total energy scores (Supporting information, Table S2). Protein–protein docking of WT CYP119 and 14 mutants of CYP119 with Pdx were performed using the RosettaDock server Rosie. The docking results of Pdx with WT and selected CYP119s are shown in Table 1 (Table S3 shows docking results for all mutants tested). The total score of models renders protein–protein interaction and internal energy of the protein. The linear combination of non-bonded atom–pair interaction energies makes up the Rosetta interface score (ISC). The total energy of the two monomeric structures is subtracted from the total energy of the complex structure to calculate this score. Stated differently, separable energy is subtracted from complex energy to determine the interface score for each scoring term. None of the mutants tested showed significant increase in the total score of interface score compared to WT CYP119. Therefore, detailed structural analysis was performed on the docked models to select mutants to continue with the experimental studies.

**Table 1.** Docking results of Pdx with WT and selected mutant CYP119s using Rosie Docking Server.

| Mutant Name | Total Score (REU) | Interface Score (REU) | RMSD (Å) |
|---|---|---|---|
| WT CYP119 | −502.7 | −3.5 | 1.5 |
| N34E | −502.6 | −3.0 | 1.1 |
| N34E/D77R | −501.1 | −3.2 | 1.6 |

Ten lowest-interface-energy structures for each run were downloaded for further analysis and visualization; the prediction accuracy of the binding site between the protein complexes was assessed. Distances between critical residues identified from structural alignment results were analyzed (Table S4). The selection of mutants for further studies involved three sequential rounds of elimination based on structural analysis of key inter-protein residue distances to predict improved electron transfer and binding affinity, ultimately favoring mutants with the D77R substitution. The goal was to mimic or improve upon the interactions observed in the well-characterized P450cam−Pdx complex. The selection process is described in Figure S3.

Based on this analysis, N34E and N34E/D77R mutants were selected for further experimental study. The schematic representation of the selected N34E/D77R CYP119 docked with Pdx is shown in Figure 1.

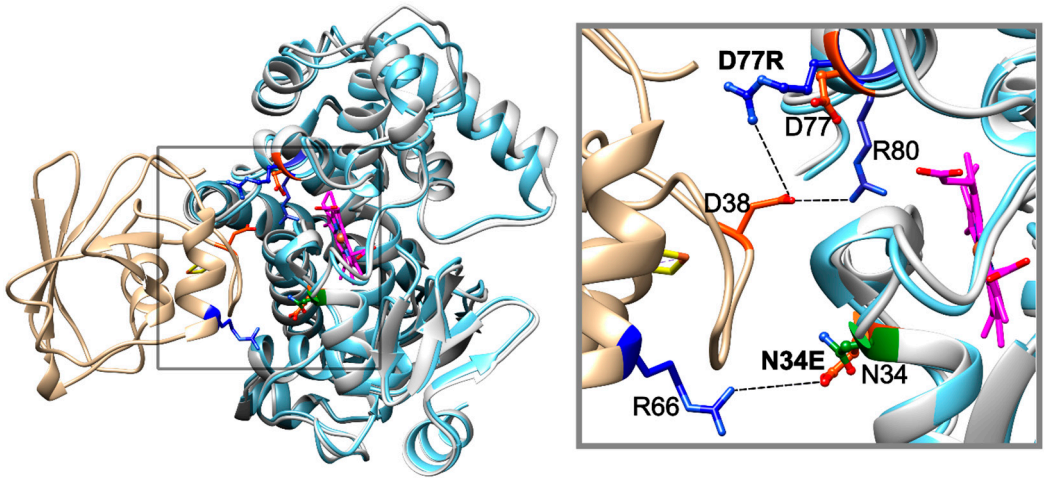



**Figure 1.** Docked structure of N34E/D77R CYP119 and Pdx showing distances between critical residues of mutant CYP119 and Pdx: N34E/D77R CYP119 (in light blue)—Pdx (in tan) complex; Arg80 (blue)-Asp38 (red), Glu34 (red)-Arg66 (blue), Arg77 (blue)-Asp38 (red) of CYP119-Pdx, heme (purple); WT CYP119 (grey): Asn34 (green), Asp77 (red), heme (purple). Images were created using UCSF ChimeraX version 1.9.1.

### *2.2. Cloning, Expression, and Purification of WT and Mutant CYP119s*

WT and mutant CYP119 proteins were cloned and expressed in *E. coli*, as described in Section 4. Protein expression was induced using 1 mM of IPTG; cells were grown at a temperature of 30 °C for 32 h [25]. Purification involved initial heat treatment of cell lysate at 60 °C followed by ammonium sulfate precipitation. Isolation and final purity of WT CYP119 were monitored by SDS-PAGE (Figure S4).

### *2.3. UV–Visible Spectral Analysis of WT and Mutant CYP119s*

Optical spectra of WT and mutant CYP119s can be seen in Figure 2. Similarly to previous observations, WT CYP119 had maximum absorbance at 415 nm and split α/β bands at 531 and 565 nm [25]. Mutations did not cause a significant shift in the maximum Soret absorbance. However, broadening in α/β bands was observed. N34E/D77R and D77R mutants showed split α/β bands at 531 and 565 nm, while the N34E CYP119 showed split α/β bands at 525 and 565 nm. Heme incorporation of N34E, N34E/D77R, and D77R mutant CYP119s were examined from the 415 nm (Soret band) and 280 nm ratio. This ratio was 0.32, 0.52, 0.53, and 0.59 for N34E, N34E/D77R, and D77R mutant CYP119s and WT CYP119, respectively. While isolated proteins showed comparable heme incorporation levels, the mutants, especially N34E, were isolated in lower purity compared to WT CYP119

(Figure S4). In all the experiments performed, enzyme concentration was based on the heme extinction coefficient to ensure CYP contents were identical.

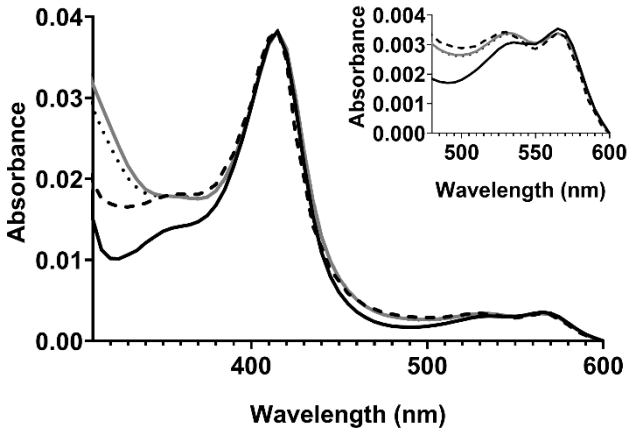



**Figure 2.** UV–Visible Spectra of WT and mutant CYP119s. Inset: the changes observed in the α/β bands. WT (black), N34E (dash), D77R (dot), N34E/D77R (grey).

### *2.4. Lauric Acid Binding to WT and Mutant CYP119s*

Lauric acid binding to WT, N34E, D77R, and N34E/D77R CYP119 was compared using difference spectroscopy; shifts in the Soret peaks of each sample were followed with increasing lauric acid concentrations. The $K_d$ of each mutant for the binding of lauric acid was similar within error relative to WT CYP119 (Table 2, Figure S5). The $K_d$ obtained for WT CYP119 was consistent with previous observations [25]. As expected, the mutations did not significantly alter the affinity for lauric acid.

**Table 2.** Effect of mutations on the binding of lauric acid and Pdx to CYP119. Pdx binding was determined in the presence of 1 mM lauric acid [1].

| Enzyme | Lauric Acid Binding $K_d$ (μM) | Pdx Binding $K_d$ (μM) |
|---|---|---|
| WT CYP119 | 19 ± 6 | 2390 ± 224 |
| N34E | 35 ± 19 | 112 ± 48 |
| D77R | 87 ± 53 | 797 ± 184 |
| N34E/D77R | 23 ± 11 | 200 ± 31 |

[1] Values are reported as the means of triplicated determinations ±SD.

### *2.5. Putidaredoxin Binding to WT and Mutant CYP119s*

The spectral shift observed in CYP119 Soret absorbance in the presence of Pdx is similar to the one observed for P450cam and Pdx [14]. The difference spectra of Pdx-bound WT CYP119 and N34E, D77R, and N34E/D77R double mutants revealed a trough at 414 nm and a peak at 440 nm for all samples. The $K_d$ obtained from difference spectra for Pdx binding for WT CYP119 was 2.4 ± 0.2 mM, while a $K_d$ of 0.11 ± 0.05 mM for N34E, 0.8 ± 0.2 mM for D77R and 0.2 ± 0.03 mM for N34E/D77R was observed (Figure 3 and Table 2). The reported $K_d$ for Pdx binding for WT and D77R CYP119 in the presence of lauric acid are 2.1 mM and 0.5 mM, respectively [14], consistent with our observations. While the D77R single mutation resulted in only a 3-fold increase in affinity, N34E and N34E/D77R mutations resulted in a 20 and 12-fold increase in affinity for Pdx, respectively.

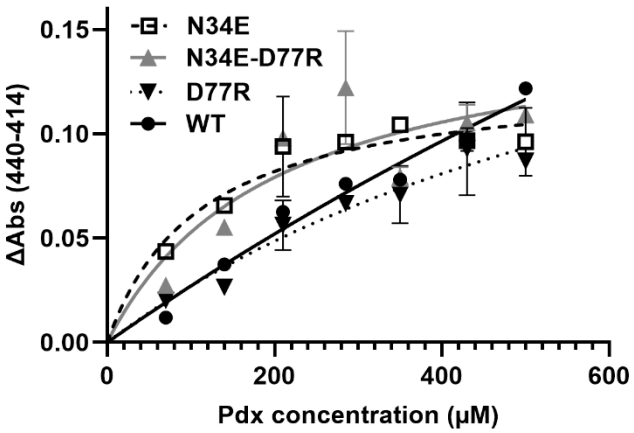



**Figure 3.** The binding of Pdx to WT, N34E, N34E/D77R and D77R CYP119 enzymes observed by difference spectra. Non-linear fitting of ΔAbs and Pdx concentration. UV–visible spectra of a solution containing 10 mM potassium phosphate (pH 7.4), 1 mM lauric acid, and 1.5 μM WT and mutant CYP119 were measured stepwise by adding Pdx (0.07–0.5 mM). The dissociation constant ($K_d$) was calculated by plotting the shift in Δ440–Δ414 against the concentration of the substrate to the quadratic equation shown in Equation (2).

### *2.6. Assessment of Electron Transfer from Putidaredoxin to WT and Mutant CYP119s*

Electron transfer capacity was determined by comparing the absorbance at 450 nm of the carbon monoxide (CO)-complex of ferrous CYP119 reduced with Pdx-PdR redox system and the control peak at 450 nm of the CO-complex CYP119 reduced with sodium dithionite using the UV–Visible spectrum (Figure 4). The final absorbance at 450 nm in the presence of redox partners was used to quantify the efficiency of CYP119 reduced by the Pdx-PdR redox system. When the Pdx-PdR redox system reduced WT CYP119, a 6.2% reduction was observed. N34E CYP119 showed an 11.4% reduction, whereas in D77R CYP119, 20.4%, and in N34E/D77R CYP119, a 45.7% reduction was observed (Table 3). While the D77R single mutant resulted in a three-fold increase in electron transfer efficiency, the N34E/D77R double mutant resulted in a seven-fold increase in electron transfer efficiency.

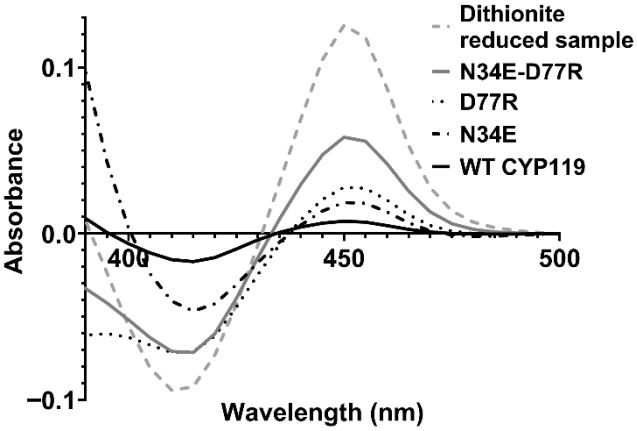



**Figure 4.** Electron transfer efficiency in WT and mutant CYP119s. The dithionite-reduced CO-difference spectrum for WT CYP119 is compared with the CO-complex spectrum after reduction by Pdx and PdR in the presence of NADH for WT, N34E, N34E/D77R and D77R CYP119. The samples contained CYP119 (2 μM) in 700 μL KPi buffer (pH 7.4), while the control cuvette contained CYP119 (2 μM) in CO-bubbled 700 μL KPi buffer (pH 7.4). Reductions were performed with (1) sodium dithionite; (2) with redox partners Pdx and PdR at an optimized ratio of 1:10:2—CYP119:Pdx:PdR (2 μM CYP119, 20 μM Pdx and 4 μM PdR) in KPi buffer (pH 7.4). NADH (0.5 mM) was added to initiate the reaction.

**Table 3.** Concentrations of CO-complexed reduced CYP119 proteins. Reduced proteins (%) are calculated by taking the ratio of the observed CO-bound CYP119 concentration reduced with redox partners, Pdx and PdR, to the observed CO-bound CYP119 concentration obtained by samples reduced with sodium dithionite [1].

| Enzyme | Concentration (μM) | Reduced (%) |
|---|---|---|
| WT CYP119 | 0.09 ± 0.007 | 6.2 |
| N34E | 0.22 | 11.4 |
| D77R | 0.31 ± 0.08 | 20.4 |
| N34E/D77R | 0.63 ± 0.1 | 45.7 |

[1] Values are reported as the means of triplicated determinations ±SD.

### *2.7. Fatty Acid Hydroxylation of WT and N34E/D77R CYP119*

CYP119 catalyzes the hydroxylation of lauric acid in the presence of Pdx, PdR, and NADH, using an optimized enzyme ratio of 1:20:1 for CYP119:Pdx:PdR. Catalase was included to decompose $H_2O_2$ from uncoupling and prevent peroxide-driven reactions. The substrate and reaction products were analyzed by GC-FID after extraction and derivatization. GC-FID analysis showed the formation of one main product by WT and N34E/D77R mutant (Figure S6A). The main product was identified as 11-hydroxylauric acid by GC-MS analysis (Figure S7) [14]. Since 12-hydroxylauric acid was not observed as a product, it was added to samples as an internal standard to reduce errors in the quantification of lauric acid (Figure S6B). The N34E/D77R mutation resulted in a 45% increase in activity based on lauric acid consumption (Figure 5).

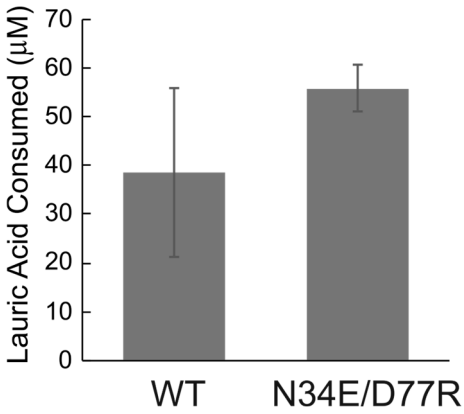



**Figure 5.** Lauric acid hydroxylation activity of WT and N34E/D77R CYP119. Lauric acid hydroxylation with CYP119 with redox partners Pdx and PdR at an optimized ratio of 1:20:1—CYP119:Pdx:PdR (0.5 μM CYP119, 10 μM Pdx and 0.5 μM PdR) in the presence of 1 mg/mL catalase. NADH (3 mM) was added to initiate the reaction.

### *2.8. Investigation of Uncoupling and Electron Transfer of WT and Mutant CYP119s*

In CYP reactions, when the electrons are transferred to oxygen instead of the substrate, superoxide anion or hydrogen peroxide can be formed instead of the product. These reactive oxygen species can then be further reduced to water. This process is called uncoupling. Despite the consumption of NADH, the reaction does not lead to the desired product; furthermore, the reactive oxygen species can react with amino acids and inactivate the enzyme. Enhanced electron transfer between redox partners is expected to reduce uncoupling and increase the efficiency of the reaction. Ampliflu™ Red assay described by Morlock et al. was used to investigate the effects of mutations on the uncoupling of the CYP119 and mutant reactions with Pdx and PdR. Briefly, the hydrogen peroxide production during the reaction is quantified using Ampliflu™ Red (50 μM) and HRP (0.2 U) [15]. During reaction

with the CYP119 system, significant superoxide production was also observed, necessitating the addition of excess SOD in addition to HRP. The enzyme ratio was optimized to 2:10:1 for CYP119:Pdx:PdR during this assay. The changes in the UV–Visible spectra were monitored for 2 h at room temperature after initiation of the reaction by the addition of NADH (50 μM). The UV–Visible spectra and the difference spectra observed during the reaction are shown in Figure S8. The formation of hydrogen peroxide was observed by following resorufin formation at 570 nm, and the decrease in NADH concentration was observed at 340 nm as previously described. In addition, there was a concurrent decrease in 420 nm and 450 nm after the initial addition of NADH, which recovered with time. The difference spectra allowed identification of this peak as oxidized Pdx. The changes in 570 nm did not follow simple kinetics due to the fact that electron transfer between PdR and Pdx is much faster than Pdx and CYP119. As seen from the changes in 450 nm, during the depletion phase of NADH, most of Pdx is in the reduced state. After NADH consumption reaches an equilibrium Pdx, oxidation reaches a steady state, where Pdx is oxidized and reduced at the same rate. The initial phase of resorufin formation is rapid and shows complicated kinetics (Figure S9). However, once oxidized Pdx has reached steady state, absorbance at 570 nm shows a linear increase in time (Figure 6). In the presence of CYP119, an increase in the formation of resorufin is observed, since the peroxide shunt of CYPs also produces superoxide. Since lauric acid is not the enzyme's natural substrate, an increase in hydrogen peroxide production is observed even in the presence of lauric acid. N34E/D77R and D77R mutants increased resorufin formation. The presence of lauric acid did not affect resorufin formation in WT; however, significant decreases in the resorufin formation were observed for D77R and N34E/D77R mutants in the presence of lauric acid. Therefore, the mutations increased the coupling efficiency as expected. In the absence of lauric acid, the rate of resorufin formation in the second phase is expected to be proportional to the electron transfer rate to CYP119 from reduced Pdx. This rate was obtained as $3.9 \times 10^{-2}$ μM $min^{-1}$, $1.2 \times 10^{-1}$ μM $min^{-1}$, $7.9 \times 10^{-2}$ μM $min^{-1}$ for WT, D77R and N34E/D77R, respectively.

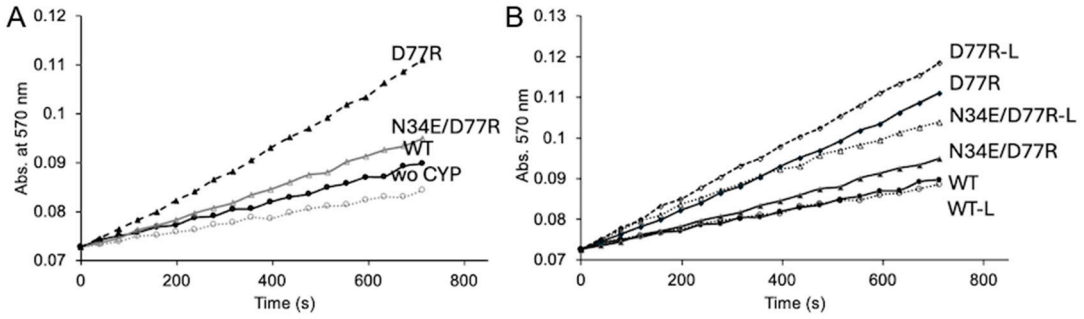



**Figure 6.** Time course of resorufin formation after steady state of Pdx oxidation is reached. (**A**) Comparison of resorufin formation for WT, D77R, and N34E/D77R mutants of CYP119 with respect to no CYP present in the presence of lauric acid (200 μM). (**B**) Resorufin formation in the presence and absence of lauric acid for WT, D77R, and N34E/D77R mutants of CYP119. (-L denotes absence of lauric acid). Hydrogen peroxide production measured with the Ampliflu™ Red assay in the reaction of WT and mutant CYP119s (1 μM) in the presence of Pdx (5 μM) and PdR (0.5 μM) under the standard conditions (50 mM sodium phosphate buffer, pH 7.4, 50 μM Ampliflu™ Red, 0.2 U HRP, 20 U/mL SOD, when present 200 μM lauric acid).

## 3. Discussion

CYPs are versatile biocatalysts capable of catalyzing diverse oxidation reactions with broad industrial potential. A functional P450 system typically relies on redox partners to facilitate electron transfer from NAD(P)H to heme. Therefore, to increase the catalytic efficiency of CYPs, it is vital to optimize or reshape the electron transfer pathway [26]. The

approaches to achieving this result can be listed as focusing on electron supply, selecting suitable redox partners, and enzyme engineering [7]. For example, truncation of the redox partner adrenodoxin (Adx) resulted in a 20-fold increased efficiency in the formation of bovine CYP11B1-dependent hydrocortisone [27]. Another mutant of truncated Adx with higher similarity to Pdx enhanced the activity of formation of CYP11B1-dependent corticosterone 3-fold, and the same mutant improved conversion of CYP11A1-dependent cholesterol by 75-fold [28]. These impressive examples demonstrate that by optimizing the redox partner affinities, it is possible to increase the yield of products substantially.

The thermophilic CYP119 can accept electrons from Pdx and PdR, originally native redox partners for P450cam [18]. Improved electron transfer to CYP119 from Pdx can be obtained by creating a more favorable protein–protein interaction [29]. Such an example is the D77R mutation on CYP119 made by Koo et al. (2002), which increased the electron transfer rate 5-fold compared to WT CYP119 by using the alignment of CYP119 and P450cam proteins [14]. In addition, the D77R mutation did not impact the enzyme's thermostability, nor did the mutation affect the $K_d$ values of the tested substrates [14].

Inspired by Koo et al., we hypothesized that CYP119 and Pdx interaction can be improved by mutations obtained from detailed structural analysis of CYP119 docked to Pdx. Previous results showed that the key residue in the electron transfer of the P450cam-Pdx complex, Arg112, corresponds to Arg80 in CYP119 [30]. It is expected that in the CYP119-Pdx complex, Arg80 also would play a vital role in the electron transfer system, forming a salt bridge with the Asp38 residue of Pdx. The alignment of two proteins, CYP119 and P450cam, shows that Asp77 of CYP119 corresponds to Arg109 of P450cam, a vital residue for P450cam-Pdx association [31]. Therefore, these residues and the distances between them were one of the main factors in selecting mutants for further experimental studies.

Amino acid residues of P450cam, Glu76, and Asp77 connect with the electropositive side of Pdx with the Arg66 residue. These residues are important in P450cam-Pdx binding. Glu76 and Asp77 correspond to Asn34 and Asn35 residues in CYP119, respectively, giving the idea to create mutations of Asn34 or Asn35 residues, changing them to negatively charged residues either Glu or Asp, so they can also form a salt bridge with Arg66 residue of Pdx. Mutation of Lys30 of CYP119 to Glu or Asp was also investigated as this residue may interact with Arg66 of Pdx. Rather than on the distal side, where substrate-binding occurs, Asn34 and Asp77 are found on the proximal surface region of the protein. Therefore, the mutations of current residues were not anticipated to affect the lauric acid affinity of the enzyme, as evidenced by the fact that no significant changes were observed for $K_d$ of lauric acid in any of the mutants tested (Table 2). All selected residues were non-conserved and located in the surface area of the binding site of CYP119 to Pdx.

PyRosetta 3 Software [32] was used for the computational prediction and design of proteins. The total energy of WT CYP119 calculated by PyRosetta was −675.3 REU, while total energies of mutant CYP119s ranged between −675.6 REU (K30E) and −706.5 REU (N34D/N35D) (Table S2), showing that all mutants were more stable compared to WT CYP119. Protein–protein docking of WT and mutant CYP119s with partner protein Pdx were also performed using PatchDock, ClusPro, HawkDock, Prism, and ZDock servers. The servers listed above are fast and allow for global docking searches; however, models are not accurate at the atomic level [33,34]. Therefore, the RosettaDock Server was used to obtain more accurate results.

EMBL PISA analysis was applied to P450cam-Pdx (PDBID: 4JWS) and docked WT CYP119-Pdx, N34E CYP119-Pdx, and N34E/D77R CYP119-Pdx complexes to understand important interactions between the CYPs and Pdx [35]. For the P450cam-Pdx interface, one salt bridge is identified between Arg112 and Asp38. In addition, five residues of

P450cam were involved in H-bonds with Pdx; Glu76, Asn116, Arg109, Asp125, Arg112. In all CYP119 structures (WT and mutants), the Arg80 and Asp38 salt bridge is preserved. In WT CYP119, an additional H-bond is formed between Gln90 of CYP119 and Gly31 of Pdx; this H-bond is lost in the mutant structures. Even though the N34E mutation was designed to generate an H-bond between Glu34 and Arg66 of Pdx, this bond was not identified in the analysis of N34E and N34E/D77R Pdx complexes. The distance between these residues is 4.69 Å, which is longer than 4 Å, which is the limit of PISA analysis. A dynamic analysis of the interface, which allowed different conformations, would likely identify the expected H-bonding interaction. In the N34E/D77R CYP119-Pdx complex, Arg77 forms two H-bonds with Trp106 and Gln105 of Pdx. In addition, the P450cam-Pdx complex has the largest number of interfacing residues, as expected: 17 residues from P450cam and 19 residues from Pdx. Interestingly, the N34E mutant has the largest interface surface area and the highest number of interfacing residues (Table S5) compared to the WT and N34E/D77R mutant. Overall, interface analysis supports our hypothesis that both N34E and N34E/D77R mutants have a stronger interaction with Pdx compared to WT CYP119.

Detailed analysis of the docked structures and literature analysis resulted in the selection of three mutations: N34E, N34E/D77R, and D77R. The site-directed mutagenesis method was applied to create these mutations. To understand if the designed mutations resulted in increased affinity of CYP119 to Pdx, Pdx binding to WT and mutant CYP119 was investigated. The reported $K_d$ for Pdx binding for WT and D77R CYP119 in the presence of lauric acid are 2.1 mM and 0.5 mM, respectively [14], consistent with our observations. The $K_d$ for Pdx binding for WT showed 2.4 $\pm$ 0.2 mM, while 0.11 $\pm$ 0.05 mM for N34E, 0.8 $\pm$ 0.2 mM for D77R and 0.2 $\pm$ 0.03 mM for N34E-D77R. These results provide direct evidence that the N34E, N34E/D77R mutants bind to Pdx with higher affinity. Thus, the increasing binding affinity of Pdx to CYP119 increased 20-fold in the N34E mutation and 12-fold in the N34E-D77R mutation (Table 2). D77R mutation confirmed around a 3-fold increase in binding, as suggested by Koo et al. (2002) [14].

The results obtained after the alignment method of the crystal structure of Pdx and the generated docked structures are feasible docking arrangements that are compatible with all the currently existing data in the literature. CYPs recognize and bind small molecule substrates considerably differently than they bind proteins. It is anticipated that the electron transfer proteins will be attached to the CYPs on a flat surface from the proximal face of the heme. On the other hand, the substrates bind in the heme's protein cavity on the distal side. Consequently, these results imply that the alignment of proteins utilized to identify the interacting surface residues and the assumption of a conserved docking region for Pdx on CYP119 were both appropriate. These findings are confirmed by the dissociation constants for Pdx's binding to CYP119, demonstrating that the N34E and N34E/D77R mutants bind to Pdx with greater affinity.

Our results show that the N34E mutant exhibits a 20-fold increase in Pdx binding affinity compared to WT CYP119. Based on this, we designed a double mutant, N34E/D77R, building on previous findings that the D77R mutation enhances electron transfer [14]. Indeed, the N34E/D77R mutant displayed fourfold higher affinity for Pdx compared to D77R alone. Under equilibrium conditions, the N34E/D77R mutant showed a twofold increase in NADH-dependent CYP reduction relative to the D77R mutant (Table 3). However, lauric acid hydroxylation by N34E/D77R showed only a 45% increase in activity over WT CYP119 (Figure 5), whereas the D77R single mutant had previously shown a threefold increase [14].

The coupling efficiency of the mutants and WT CYP119 was also investigated by monitoring $H_2O_2$ formation to understand the differences in electron transfer rates between mutants. The sample with redox partners without CYP was used as a control. When

CYP is absent, NADH reduces PdR, and PdR transfers electrons to Pdx. However, Pdx has no terminal electron acceptor to pass them to. The reduced Pdx might pass electrons back to PdR (thermodynamically uphill, but possible). Eventually, PdR will transfer electrons to molecular oxygen via Pdx, producing reactive oxygen species (ROS) like superoxide ($O_2^{-}\bullet$) or hydrogen peroxide ($H_2O_2$). In the Ampliflu™ Red assay, superoxide was converted to hydrogen peroxide and water by excess SOD, which was followed by resorufin formation. Hydrogen peroxide production was expected to be lower in the presence of CYPs since they accept electrons from Pdx and reduce the substrate. In the CYP catalytic cycle, substrate binding is followed by an electron transfer from NAD(P)H to the heme center, enabling oxygen binding. The oxygen is reduced to a ferric peroxy anion, then cleaved with two protons to release water and form the reactive "oxenoid" complex. This activated oxygen atom is inserted into the substrate. Alternatively, reactive oxygen species (ROS) such as superoxide or hydrogen peroxide can form from decay of the iron-oxygen intermediates. Since lauric acid is not the native substrate for CYP119, significant uncoupling and production of ROS were observed in the presence of CYP119. Since the electron transfer from Pdx to CYP119 is more rapid than the electron transfer from Pdx to oxygen, the addition of CYP119 resulted in an increase in $H_2O_2$ production rate during the steady state of Pdx reduction. Faster electron transfer between CYP and Pdx resulted in higher hydrogen peroxide production and increased resorufin formation (Figure 6A). The difference in resorufin formation in the absence and presence of substrate is another indicator of uncoupling. For WT CYP119, the presence of substrate did not affect resorufin formation rate at all, indicating very high levels of uncoupling. Both D77R and N34E/D77R mutants showed decreased hydrogen peroxide production in the presence of lauric acid (Figure 6B); therefore, both mutants show increased coupling efficiency.

In the Ampliflu™ Red assay without substrate lauric acid, electrons transferred from Pdx to CYP119 will lead to $H_2O_2$, which oxidizes Ampliflu™ Red to form resorufin. The electron transfer from Pdx to CYP119 mutants can be observed indirectly through the resorufin formation via the mechanism described above. D77R single mutant showed a three-fold increase in resorufin formation rate compared to WT CYP119 in the absence of lauric acid (Figure 6). This result is consistent with previous studies where a five-fold increase in the electron transfer rate is observed for D77R CYP119 [14]. However, the N34E/D77R double mutant shows only a two-fold increase in resorufin formation compared to the WT; the rate of resorufin formation is lower for the N34E/D77R mutant compared to the D77R mutant. Therefore, the N34E mutation lowered the electron transfer rate, even though it increased the affinity for Pdx.

The effects of the N34E mutation on the surrogate redox system for CYP119 can be understood by a more detailed analysis of the electron transfer mechanism. The first electron transfer is likely to occur in two steps, as shown in reactions 1 and 2, where $Pdx^{r}$ denotes the reduced form of Pdx and $Pdx^{ox}$ denotes the oxidized form.

$$CYP119^{3+} + Pdx^{r} \rightleftarrows CYP119\bullet Pdx \quad (1)$$

$$CYP119\bullet Pdx \xrightarrow{k_1} CYP119^{2+} + Pdx^{ox} \quad (2)$$

The D77R mutant increases both binding affinity ($K_a$) and electron transfer rate ($k_1$), resulting in a significant improvement in overall electron transfer and catalytic activity. In contrast, the N34E mutation increases $K_a$, it likely reduces $k_1$, leading to a lower electron transfer rate. As a result, the combined N34E/D77R mutant shows only a modest increase in activity. The introduction of a negative charge at the Pdx binding interface by the N34E mutation may interfere with efficient electron transfer between the two proteins.

In the case of the N34E CYP119, while the docking analysis indicated that the N34E mutant brings the redox cofactors slightly closer (16.7 Å vs. 18.3 Å in WT CYP119–Pdx), electron transfer activity was nonetheless reduced, suggesting that distance alone is not the limiting factor. The introduction of a negatively charged residue at position 34 likely perturbs the local electrostatic environment at the interface, potentially over-stabilizing the complex or altering the reorganization energy required for efficient electron transfer. Similar observations have been reported for CYP–redox partner systems, where enhanced electrostatic attraction leads to tighter binding but diminished electron flow due to decreased conformational flexibility and impaired formation of transient, catalytically competent states [22,36–38]. Moreover, studies on P450cam and its redox partner putidaredoxin have shown that productive electron transfer depends on a dynamic equilibrium between bound and dissociated states rather than static complex stabilization [37,38]. In addition, mutations in Pdx that significantly decreased binding affinity for ferric P450cam did not correspondingly reduce the first electron transfer rate, suggesting that factors beyond binding affinity influence electron transfer efficiency [23,39,40]. Thus, the N34E mutation may lock the complex into a non-optimal, rigid configuration—favoring affinity over the transient dynamics required for rapid electron exchange.

The effect of the D77R mutation on $k_1$, the electron transfer rate, is supported by previous observations. The Asp77 in CYP119 corresponds to Arg109 in P450cam; Arg109 is a crucial residue in electron transfer between P450cam and Pdx. Mutations in Arg109 resulted in a significant increase in uncoupling [21]. In addition, Arg109 maintains an H-bond with Trp106 of Pdx. Previous studies have shown that Trp106 is crucial for electron transfer, as W106A Pdx is completely inactive [34]. Our PISA analysis confirms H-bond formation between Arg77 and Trp106 in the N34E/D77R mutant-Pdx complex.

These findings underscore the complexity of engineering electron transfer in CYP systems. While we successfully engineered the CYP119 interface to achieve a novel variant with a 20-fold increase in Pdx binding affinity, our catalytic assays revealed a critical, non-obvious relationship: stronger binding does not necessarily translate to improved electron transfer efficiency or catalytic turnover. The observed decoupling between binding strength and electron-transfer rate highlights the need for a more nuanced understanding of the structural and dynamic factors governing P450 catalysis. This insight provides a valuable foundation for optimizing electron flow in CYP-based biocatalysts through balanced interface design rather than solely affinity-driven mutations.

Beyond improving native systems, our results also inform the construction of artificial redox partner networks and hybrid P450 systems with tunable electron delivery—an essential step toward developing self-sufficient or light-driven P450 catalysts. Future work integrating computational electron-transfer pathway analysis, time-resolved spectroscopy, and directed evolution can expand these findings to other CYP families and guide the rational engineering of next-generation P450 enzymes. Such advances will enhance the sustainable biosynthesis of high-value products, including pharmaceuticals (e.g., cortisone, pravastatin, artemisinic acid) and agrochemicals, while deepening our mechanistic understanding of biological electron transfer.

## 4. Materials and Methods

### *4.1. Materials*

The pET11a containing wild type (WT) CYP119, the pET28b containing putidaredoxin (Pdx) and putidaredoxin reductase (PdR) were gifts from Teruyuki Nagamune (Addgene plasmid #66131, #85084, #85083, respectively) [9,41].

### *4.2. Design of CYP119 Mutant Enzymes and Protein–Protein Docking*

PyRosetta 3 Software was used in designing the mutants according to the protocol described by Kestevur Dogru et al. (2023) [42]. Docking2 protocol (Local_Docking_Refine) of RosettaDock server Rosie1 was used for the protein–protein docking experiment [31,32,40]. It necessitates two different protein structures as an input in a standard pdb format with starting configuration and coordinates. Single mutants N34D, N34E, N35D, N35E, K30D, K30E, double mutants N34D/D77R, N34E/D77R, N35D/D77R, N35E/D77R, K30D/D77R, K30E/D77R, N34E/N35D, N34D/N35D and Pdx (PDBID: 1XLN) were submitted to dock using RosettaDock server Rosie in two separate pdb files. The coordinates of the two proteins were not overlapping and docking partners Cα atoms were distanced from each other for higher than 5 Å to avoid a collision. Ten lowest-interface-energy structures were created in each docking run and downloaded for further analysis and visualization. Obtained complexes were aligned with the P450cam-Pdx crystal structure (with PDB id: 4JWS) and WT CYP119 (PDB id: 1IO7)-Pdx complex to assess the prediction accuracy of the binding site of CYP119 mutant-Pdx complexes and its correlation with these complexes. Designed mutants' protein–protein interactions were analyzed by the PISA program [33].

### *4.3. Cloning, Expression, and Purification of WT and Mutant CYP119s*

Site-directed mutagenesis of CYP119 was performed using the Q5 Site-Directed Mutagenesis Kit. The forward and reverse primers used for N34E mutation are, respectively, (mutated region is labeled in boldface), 5′-GGAGGTTTTA**GAG**AACTTTTCGAAATTC-3′ and 5′-CAAAAGGATATCCATGTGTTT-3′, and for D77R mutation: 5′-CCCTCTCCAT**CGT**GA GTTAAGATCAATG-3′ and 5′- GTACGACTGGAGTCTAGG-3′. WT and mutant proteins were expressed according to Baslar (2020) [25]. A single colony was grown overnight at 37 °C, 220 rpm in 100 mL of Lysogeny Broth (LB) medium with 0.1 mg/L ampicillin. The overnight cells (5 mL) were placed into 500 mL 2xYT medium (16 g/L tryptone, 10 g/L yeast extract, and 5 g/L NaCl at pH 6.8) and incubated at 37 °C, 220 rpm, until CYP119 had an $OD_{600}$ of 0.8. Protein expression was induced with 1 mM of IPTG, and cells were grown at 30 °C for 32 h. Cell pellets were harvested by centrifugation for 30 min at 3900 g. Proteins were purified, according to Sakalli (2022) [43]. Frozen cell pellets (1 g) were dissolved in Lysis buffer (5 mL) (50 mM potassium phosphate buffer (KPi), 150 mM NaCl, 0.2 mM phenylmethylsulfonyl fluoride (PMSF), 1 mM benzamidine HCl, 10 mM imidazole (pH 7.5)) and sonicated for 30 s, then the cells were kept on ice for a minute. Sonication was performed until the cells were lysed. Lysate was incubated for 1 h at 60 °C in a water bath and centrifuged at 3900 rpm for 1.5 h. The supernatant was subjected to 30% and 60% ammonium sulfate precipitation. Proteins were harvested by centrifugation at 3900 rpm for 90 min at 8 °C and dissolved and dialyzed against the buffer (50 mM KPi, 20 mM NaCl, 5% glycerol).

### *4.4. Expression and Purification of Redox Partners Putidaredoxin and Putidaredoxin Reductase*

*E. coli* BL 21 (DE3) cells containing pPdx and pPdR plasmids were grown according to the method by Suzuki et al. (2016) in 5 mL of LB medium containing 1% glucose, 0.05 mg/L kanamycin [41]. The cells were grown at 37 °C until $OD_{600}$ attained 0.5, around 4–5 h. The cell culture was shaker-grown in 500 mL of Terrific Broth (TB) media (12 g/L tryptone, 24 g/L yeast extract, 5 g/L glycerol) with 0.05 mg/L kanamycin at 37 °C and 220 rpm. When the $OD_{600}$ reached 0.8, 0.5 mM of $FeCl_3$ was added to pPdx plasmid-containing cells, while 0.1 mM IPTG was added to pPdR plasmid-containing plasmid-containing cells, while 0.1 mM IPTG was added to pPdR plasmid-containing cells and cell cultures were grown at 27 °C, 220 rpm shaker overnight. The cells were extracted by centrifugation at 3200× *g* for 40 min.

Putidaredoxin (Pdx) was purified according to the method by Suzuki et al. (2016) [38]. Pdx-expressing cells were dissolved using lysis buffer (150 mM KCl, 10 mM imidazole, 1 mM benzamidine HCl, 0.2 mM PMSF, 20 mM KPi pH 7.4) and sonicated for 30 s. Cell debris was removed at 3200 rpm for 40 min centrifugation, and resin (1 mL to each 8 mL of supernatant) was added to the supernatant and incubated for 1 h at 4 °C using a rotator. Lysate was then applied to the nickel-nitrilotriacetic acid (Ni-NTA) column. The column was washed with wash buffer (20 mM KPi, 20 mM imidazole pH 7.4), then elution was carried out with 5 mL of elution buffer (150 mM KCl, 300 mM imidazole, 20 mM KPi at pH 7.4). The obtained protein was dialyzed against 20 mM KPi pH 7.4, containing 5% glycerol. The purified Pdx was stored at −80 °C until use.

Putidaredoxin reductase (PdR) was purified according to protocol by Koo et al. (2002) and Suzuki et al. (2016) [14,41]. Harvested cells were lysed with lysis buffer (150 mM KCl, 10 mM imidazole, 1 mM benzamidine HCl, 0.2 mM PMSF, 20 mM KPi) and sonicated for 30 s, followed by 1 min incubation on ice. Sonication was performed until cells were lysed, and cell lysate was centrifuged at 3200 rpm for 40 min. The supernatant was subjected to 30% and 70% ammonium sulfate cuts. PdR cell pellets were dissolved in lysis buffer, and 1 mL resin was added to each 8 mL supernatant and rotated for 1 h at 4 °C. Lysate was then applied to a 5 mL Ni-NTA column. The column was washed with wash buffer (20 mM KPi, 20 mM imidazole), then proteins were eluted with 5 mL of elution buffer (150 mM KCl, 300 mM imidazole, 20 mM KPi). The dialysis was performed against 20 mM KPi buffer at pH 7.4, containing 5% glycerol. The purified PdR was stored at −80 °C until use [9].

### *4.5. UV–Visible Spectral Analysis of WT and Mutant CYP119s*

WT and mutant CYP119s in 50 mM KPi at pH 7.5 were examined under the UV–visible spectra. Scanning Spectrophotometer 1600PC (VWR International, Shanghai, China) was utilized for analysis. Optical spectra of each sample were recorded. CYP119 concentration was calculated using the extinction coefficient ($\varepsilon_{415nm}$ = 104 $mM^{-1}$ $cm^{-1}$) [25].

### *4.6. UV–Visible Spectral Analysis of Putidaredoxin and Putidaredoxin Reductase*

Isolated Pdx and PdR (1 μM) were examined with UV–visible spectra in 50 mM KPi at pH 7.4. UV–visible spectroscopy was carried out using a 1600PC Scanning Spectrophotometer. The concentration of Pdx was calculated using its known extinction coefficient ($\varepsilon_{412nm}$ = 11.0 $mM^{-1}$ $cm^{-1}$) at 412 nm [11]. The concentration of PdR was calculated from its extinction coefficient at 455 nm ($\varepsilon_{455}$ = 10.9 $mM^{-1}$ $cm^{-1}$) [44]. Alternatively, extinction coefficient $\varepsilon_{378}$ = 9700 $M^{-1}$ $cm^{-1}$ and $\varepsilon_{454}$ = 10,000 $M^{-1}$ $cm^{-1}$ for PdR can be used [11].

### *4.7. Lauric Acid Binding to WT and Mutant CYP119s*

Binding constants of WT CYP119 and mutants N34E, D77R, and N34E/D77R with the substrate, lauric acid, have been identified using difference spectroscopy. All experiments were performed at room temperature. Samples contained 1.5 μM enzyme in 50 mM KPi buffer at pH 7.4. An overall volume of 7 mL was divided into two glass cuvettes, each 3.5 mL, after incubating samples for 10 min. Lauric acid stock in dimethyl sulfoxide (DMSO) was added stepwise with final concentrations (0, 10 μM, 20 μM, 30 μM, 40 μM, 50 μM, 80 μM, 110 μM, 140 μM, 170 μM, 200 μM) to the enzyme's solution and incubated for 5 min at room temperature before UV–visible spectra were taken. Reference cuvettes contained the samples where the substrate volume of DMSO was added. The final DMSO concentration was less than 1% of the total volume of the solution. UV spectra of all samples were measured between 350 nm and 650 nm, and the absorbance shift was fol-

lowed between 386 nm and 418 nm. Next, by fitting plots of Δ386–Δ418 against substrate concentration to Equation (3), the dissociation constant ($K_d$) was calculated.

$$\Delta A = A_{max}\left(\frac{K_d + [E] + [L] - \sqrt{(K_d + [E] + [L])^2 - 4[E][L]}}{2[E]}\right) \quad (3)$$

*4.8. Putidaredoxin Binding to WT and Mutant CYP119s*

UV–visible spectra of the total volume of 700 µL solution containing 10 mM KPi buffer (pH 7.4), 1 mM lauric acid, and 1.5 µM WT or mutant CYP119 were measured. The reference cuvette contained the same solution except for WT or mutant CYP119 enzymes. Pdx of 0.5 mM was added stepwise to both cuvettes from 70 µM to 500 µM final concentration. Difference spectra were measured between 200 and 750 nm, and the absorbance shift was followed between 440 nm and 414 nm. The dissociation constant ($K_d$) was calculated by plotting the shift in Δ440–Δ414 against the substrate concentration to the quadratic equation shown in Equation (3).

*4.9. Assessment of Electron Transfer from Putidaredoxin to WT and Mutant CYP119s*

The efficiency of the electron transfer between Pdx and CYP119 (WT or mutants) was determined by comparing the absorbances at 450 nm of the CO (carbon monoxide)-complex of WT or mutant CYP119 reduced with the Pdx-PdR redox system, with the CO-complex of CYP119 reduced with sodium dithionite. Reference cuvette contained CYP119 (2 µM) in 700 µL KPi buffer (pH 7.4), while control cuvette contained CYP119 (2 µM) in CO-bubbled 700 µL KPi buffer (pH 7.4). Solid sodium dithionite (around 0.5–1 mg solid per milliliter of the microsomal mixture) was added to the solution to convert the ferric form of CYP119 into the ferrous form and gently mixed by pipetting. The CO treatment of KPi buffer was conducted at 1 bubble/s speed for 30 min prior to reduction with sodium dithionite.

Sample cuvette contained CYP119, mixed with redox partners Pdx and PdR at an optimized ratio of 1:10:2—CYP119:Pdx:PdR (2 µM CYP119, 20 µM Pdx and 4 µM PdR) in phosphate buffer (pH 7.4). NADH was added to achieve a final concentration of 0.5 mM [45]. The CO treatment of KPi buffer was conducted at 1 bubble/s speed for 30 min prior to reduction with NADH. The reduced CYP119 concentration in the sample was determined using Equation (4), rearranged from Beer's Law (A = εcl), where $(\Delta A450 - A490)$reduced, CO—absorbance at (450–490 nm) when reduced using dithionite, CO [46].

$$\frac{\Delta(\text{A450} - \text{A490})\text{reduced, CO}}{91\frac{\mu\text{mol}}{\text{mL}} \times 1\text{cm}} \times 1000\frac{\text{nmol}}{\mu\text{mol}} = \frac{\text{nmolCYP119}}{\text{mL}} \quad (4)$$

*4.10. Fatty Acid Hydroxylation of WT and N34E/D77R CYP119*

CYP119 (500 nM) was mixed with 10 µM Pdx, 500 nM Pdr, 1 mg/mL catalase, and 200 µM lauric acid in 500 µL of 50 mM phosphate buffer (pH 7). NADH was added to start the reaction at a final concentration of 3 mM. The reaction mixtures were incubated at 37 °C for 30 min. The reactions were stopped by adding 500 µL of 6% HCl. The solution was incubated on ice for 10 min, and 12-hydroxydodecanoic acid (10.8 µg) was added as an internal standard. The reaction suspension was extracted (3 × 500 mL ethyl acetate), and the organic phase was evaporated. The dried organic extracts were derivatized by the addition of BSTFA (15 µL) and dry ethyl acetate (35 µL) and incubation at 60 °C for 2 h. The trimethylsilyl (TMS) derivatives were subjected to GC-FID. GC-FID analyses were carried out using an 6890N gas chromatograph (Agilent Technologies, Santa Clara, CA, USA) equipped with a flame ionization detector (FID) and an injector in combination with 7683 Series autosampler (Agilent Technologies, Santa Clara, CA, USA). An HP-5 column (30 m × 320 µm, 0.25 µm film thickness; J&W Scientific, Agilent Technologies, Santa Clara,

CA, USA) was used, with helium as the carrier gas. Samples were injected with a split ratio of 10, at an injector temperature set to 280 °C, the detector temperature was 320 °C, and the injection volume was 0.5 µL. The oven temperature was initially set to 70 °C and held for 1 min, then ramped quickly to 190 °C at a rate of 15 °C/min. This was followed by a slower increase to 250 °C at 2 °C/min, and finally a rapid rise to 300 °C at 15 °C/min, where it was held for 2 min. Lauric acid, 12-hydroxydodecanoic acid (12-hydroxylauric acid), and 11-hydroxydodecanoic acid (11-hydroxylauric acid) eluted at 10.4, 15.5, and 16.2 min. The identity of the main product, 11-hydroxylauric acid, was confirmed by GC/MS analysis. Lauric acid was quantified using standard solutions.

### *4.11. Investigation of Uncoupling and Electron Transfer of WT and Mutant CYP119s*

Ampliflu™ Red assay described by Morlock et al. was used to investigate the effects of mutations on the uncoupling of the CYP119 and mutant reactions with Pdx and PdR [15]. The assay included the following: 1 µM WT or mutant CYP119, 5 µM Pdx, 0.5 µM PdR, when present, 200 µM lauric acid, 20 U/mL superoxide dismutase (SOD), as well as 50 µM Ampliflu™ Red and 0.2 U horseradish peroxidase (HRP) in 50 mM Kpi buffer pH 7.4, and controls included the same mixture, except for CYP119 and except for substrate (lauric acid). The reaction was initiated by the addition of 50 µM NADH [14,44]. UV–visible spectra between 300–600 nm were measured with an interval of 10 nm on a 96-well plate reader for 2 h at room temperature with 30 s intervals.

**Supplementary Materials:** The following supporting information can be downloaded at: https://www.mdpi.com/article/10.3390/catal15101000/s1, Figure S1: A. Structural alignment of proteins: CYP119 (PDB ID:1IO7) in blue, Pdx (PDB ID:1XLN) in purple and P450cam-Pdx (PDB ID: 4JWS) in brown; Figure S2: Sequence alignment of proteins CYP119 and P450cam; Figure S3: Schematic of selection of CYP119 Mutants for Experimental Study; Figure S4: A. Isolation of WT CYP119 was monitored by SDS-PAGE; B. N34E; C. N34E/D77R; D. D77R; Figure S5: Lauric acid binding to WT and mutant CYP119s; Figure S6: GC-FID analysis of activity assays of WT and N34E/D77R CYP119 using lauric acid as substrate; Figure S7: GC-MS identification of 11-hydroxy lauric acid (11-OH LA) as the main product of CYP119 lauric acid hydroxylation; Figure S8: Spectral changes observed in the Ampliflu™ Red assay for investigation of uncoupling of CYP119 with Pdx and PdR redox partners; Figure S9: Time course of resorufin formation during the initial phase of the reaction; Table S1: Residues selected and selection criteria for mutational screening; Table S2: Total energies (REU) of WT CYP119 and created CYP119 mutants; Table S3: Docking results of Pdx with WT and mutant CYP119s using Rosie Docking Server; Table S4: Distances between key residues of docked Pdx with mutants of CYP119, compared to docked Pdx with wild type CYP119; Table S5: Interface analysis of P450cam, WT, N34E and N34E/D77R CYP119 complexes with Pdx using EMBL PISA.

**Author Contributions:** Conceptualization, N.B.S.; methodology, A.K.; formal analysis, N.B.S. and A.K.; investigation, N.B.S. and A.K.; resources, N.B.S.; writing—original draft preparation, N.B.S. and A.K.; writing—review and editing, N.B.S. and A.K.; visualization, N.B.S. and A.K.; supervision, N.B.S.; project administration, N.B.S.; funding acquisition, N.B.S. All authors have read and agreed to the published version of the manuscript.

**Funding:** This project was funded by the Izmir Institute of Technology (IZTECH) Scientific Research Council (BAP) project ID 2023IYTE-1-0012. A.K. was supported by Türkiye Scholarships program.

**Data Availability Statement:** The original contributions presented in this study are included in the article/supplementary material. Further inquiries can be directed to the corresponding author.

**Acknowledgments:** We thank the Environmental Development Application and Research Center for GC-FID and GC/MS analysis, and the Biotechnology and Bioengineering Application and Research Center at Izmir Institute of Technology for DNA sequencing analysis. We thank Müşerref Yersel Ural

for GC-FID analysis, and Tuğçe Sakallı for experimental help and critical reading of the manuscript. We also thank Ekin Kestevur Doğru for critical reading of the manuscript.

**Conflicts of Interest:** The authors declare no conflicts of interest. The funders had no role in the design of the study; in the collection, analyses, or interpretation of data; in the writing of the manuscript; or in the decision to publish the results.

## Abbreviations

The following abbreviations are used in this manuscript:

| | |
|---|---|
| WT | Wild-Type |
| SDM | Site-Directed Mutagenesis |
| IPTG | Isopropyl β-D-1-thiogalactopyranoside |
| ALA | 5-Aminolevulinic acid hydrochloride |
| Pdx | Putidaredoxin |
| PdR | Putidaredoxin reductase |
| CYP | Cytochrome P450 |
| NADH | Nicotinamide adenine dinucleotide hydrogen |
| FAD | Flavin adenine dinucleotide |
| HRP | Horseradish peroxidase |
| SOD | Superoxide Dismutase |

## References

1. Di Nardo, G.; Gilardi, G. Natural Compounds as Pharmaceuticals: The Key Role of Cytochromes P450 Reactivity. *Trends Biochem. Sci.* **2020**, *45*, 511–525. [CrossRef]
2. Urlacher, V.B.; Girhard, M. Cytochrome P450 Monooxygenases in Biotechnology and Synthetic Biology. *Trends Biotechnol.* **2019**, *37*, 882–897. [CrossRef]
3. Bernhardt, R.; Urlacher, V.B. Cytochromes P450 as promising catalysts for biotechnological application: Chances and limitations. *Appl. Microbiol. Biotechnol.* **2014**, *98*, 6185–6203. [CrossRef] [PubMed]
4. McLean. Monooxygenase, Peroxidase and Peroxygenase Properties and Mechanisms of Cytochrome P450. In *Advances in Experimental Medicine and Biology*; Hrycay, E., Bandiera, S., Eds.; Springer: Cham, Switzerland, 2015; Volume 851, Available online: http://www.springer.com/series/5584 (accessed on 1 June 2024).
5. Wei, X.; Zhang, C.; Gao, X.; Gao, Y.; Yang, Y.; Guo, K.; Du, X.; Pu, L.; Wang, Q. Enhanced Activity and Substrate Specificity by Site-Directed Mutagenesis for the P450 119 Peroxygenase Catalyzed Sulfoxidation of Thioanisole. *Chem. Open* **2019**, *8*, 1076–1083. [CrossRef]
6. Denisov, I.G.; Makris, T.M.; Sligar, S.G.; Schlichting, I. Structure and chemistry of cytochrome P450. *Chem. Rev.* **2005**, *105*, 2253–2278. [CrossRef]
7. He, J.; Liu, X.; Li, C. Engineering Electron Transfer Pathway of Cytochrome P450s. *Molecules* **2024**, *29*, 2480. [CrossRef]
8. Guengerich, F.P. Mechanisms of Cytochrome P450-Catalyzed Oxidations. *ACS Catal.* **2018**, *8*, 10964–10976. [CrossRef]
9. Suzuki, R.; Hirakawa, H.; Nagamune, T. Electron donation to an archaeal cytochrome P450 is enhanced by PCNA-mediated selective complex formation with foreign redox proteins. *Biotechnol. J.* **2014**, *9*, 1573–1581. [CrossRef] [PubMed]
10. Li, S.; Du, L.; Bernhardt, R. Redox Partners: Function Modulators of Bacterial P450 Enzymes. *Trends Microbiol.* **2020**, *28*, 445–454. [CrossRef]
11. Sevrioukova, I.F.; Garcia, C.; Li, H.; Bhaskar, B.; Poulos, T.L. Crystal structure of putidaredoxin, the 2Fe-2S component of the P450cam monooxygenase system from Pseudomonas putida. *J. Mol. Biol.* **2003**, *333*, 377–392. [CrossRef] [PubMed]
12. Chen, C.; Min, J.; Zhang, L.; Yang, Y.; Yu, X.; Guo, R. Advanced Understanding of the Electron Transfer Pathway of Cytochrome P450s. *ChemBioChem* **2021**, *22*, 1317–1328. [CrossRef] [PubMed]
13. Iyanagi, T. Roles of Ferredoxin-NADP$^+$ Oxidoreductase and Flavodoxin in NAD(P)H-Dependent Electron Transfer Systems. *Antioxidants* **2022**, *11*, 2143. [CrossRef]
14. Koo, L.S.; Immoos, C.E.; Cohen, M.S.; Farmer, P.J.; de Montellano, P.R.O. Enhanced electron transfer and lauric acid hydroxylation by site-directed mutagenesis of CYP119. *J. Am. Chem. Soc.* **2002**, *124*, 5684–5691. [CrossRef]
15. Morlock, L.K.; Böttcher, D.; Bornscheuer, U.T. Simultaneous detection of NADPH consumption and $H_2O_2$ production using the Ampliflu™ Red assay for screening of P450 activities and uncoupling. *Appl. Microbiol. Biotechnol.* **2017**, *102*, 985–994. [CrossRef]
16. Koo, L.S.; Tschirret-Guth, R.A.; Straub, W.E.; Moënne-Loccoz, P.; Loehr, T.M.; de Montellano, P.R.O. The active site of the thermophilic CYP119 from *Sulfolobus solfataricus*. *J. Biol. Chem.* **2000**, *275*, 14112–14123. [CrossRef]

17. Aoki, M.; Ishimori, K.; Morishima, I.; Wada, Y. Roles of valine-98 and glutamic acid-72 of putidaredoxin in the electron-transfer complexes with NADH-putidaredoxin reductase and P450cam. *Inorganica Chim. Acta* **1998**, *272*, 80–88. [CrossRef]
18. Tripathi, S.; Li, H.; Poulos, T.L. Structural basis for effector control and redox partner recognition in cytochrome P450. *Science* **2013**, *340*, 1227–1230. [CrossRef]
19. Chiliza, Z.E.; Martínez-Oyanedel, J.; Syed, K. An overview of the factors playing a role in cytochrome P450 monooxygenase and ferredoxin interactions. *Biophys. Rev.* **2020**, *12*, 1217–1222. [CrossRef] [PubMed]
20. Batabyal, D.; Richards, L.S.; Poulos, T.L. Effect of Redox Partner Binding on Cytochrome P450 Conformational Dynamics. *J. Am. Chem. Soc.* **2017**, *139*, 13193–13199. [CrossRef] [PubMed]
21. Liu, C.; Chen, X. Recent Advances in the Engineering of Cytochrome P450 Enzymes. *Catalysts* **2025**, *15*, 374. [CrossRef]
22. Stresser, D. Cytochrome P450 In Vitro Methods and Protocols. In *Methods in Pharmacology and Toxicology*; Yan, Z., Caldwell, G., Eds.; Humana: New York, NY, USA, 2021.
23. Shimada, H.; Nagano, S.; Hori, H.; Ishimura, Y. Putidaredoxin–cytochrome P450cam interaction. *J. Inorg. Biochem.* **2001**, *83*, 255–260. [CrossRef]
24. de Montellano, O. *Cytochrome P450 Structure, Mechanism, and Biochemistry*, 3rd ed; Springer: New York, NY, USA, 2005.
25. Başlar, M.S.; Sakallı, T.; Güralp, G.; Doğru, E.K.; Haklı, E.; Surmeli, N.B. Development of an improved Amplex Red peroxidation activity assay for screening cytochrome P450 variants and identification of a novel mutant of the thermophilic CYP119. *JBIC J. Biol. Inorg. Chem.* **2020**, *25*, 949–962. [CrossRef] [PubMed]
26. Kuznetsov, V.Y.; Poulos, T.L.; Sevrioukova, I.F. Putidaredoxin-to-cytochrome P450cam electron transfer: Differences between the two reductive steps required for catalysis. *Biochemistry* **2006**, *45*, 11934–11944. [CrossRef] [PubMed]
27. Zhang, L.; Xie, Z.; Liu, Z.; Zhou, S.; Ma, L.; Liu, W.; Huang, J.-W.; Ko, T.-P.; Li, X.; Hu, Y.; et al. Structural insight into the electron transfer pathway of a self-sufficient P450 monooxygenase. *Nat. Commun.* **2020**, *11*, 2676. [CrossRef] [PubMed]
28. Uhlmann, H.; Kraft, R.; Bernhardt, R. C-terminal region of adrenodoxin affects its structural integrity and determines differences in its electron transfer function to cytochrome P-450. *J. Biol. Chem.* **1994**, *269*, 22557–22564. [CrossRef]
29. Faro, M.; Schiffler, B.; Heinz, A.; Nogués, I.; Medina, M.; Bernhardt, R.; Gómez-Moreno, C. Insights into the design of a hybrid system between anabaena ferredoxin-NADP+ reductase and bovine adrenodoxin. *Eur. J. Biochem.* **2003**, *270*, 726–735. [CrossRef]
30. Koga, H.; Sagara, Y.; Yaoi, T.; Tsujimura, M.; Nakamura, K.; Sekimizu, K.; Makino, R.; Shimada, H.; Ishimura, Y.; Yura, K.; et al. Essential role of the $Arg^{112}$ residue of cytochrome P450cam for electron transfer from reduced putidaredoxin. *FEBS Lett.* **1993**, *331*, 109–113. [CrossRef]
31. Meng, S.; Li, Z.; Ji, Y.; Ruff, A.J.; Liu, L.; Davari, M.D.; Schwaneberg, U. Introduction of aromatic amino acids in electron transfer pathways yielded improved catalytic performance of cytochrome P450s. *Chin. J. Catal.* **2023**, *49*, 81–90. [CrossRef]
32. Lyskov, S.; Chou, F.-C.; Conchúir, S.Ó.; Der, B.S.; Drew, K.; Kuroda, D.; Xu, J.; Weitzner, B.D.; Renfrew, P.D.; Sripakdeevong, P.; et al. Serverification of Molecular Modeling Applications: The Rosetta Online Server That Includes Everyone (ROSIE). *PLoS ONE* **2013**, *8*, e63906. [CrossRef]
33. Chaudhury, S.; Lyskov, S.; Gray, J.J. PyRosetta: A script-based interface for implementing molecular modeling algorithms using Rosetta. *Bioinformatics* **2010**, *26*, 689–691. [CrossRef]
34. Lyskov, S.; Gray, J.J. The RosettaDock server for local protein-protein docking. *Nucleic Acids Res.* **2008**, *36*, W233–W238. [CrossRef]
35. Krissinel, E.; Henrick, K. Inference of Macromolecular Assemblies from Crystalline State. *J. Mol. Biol.* **2007**, *372*, 774–797. [CrossRef]
36. Follmer, A.H.; Tripathi, S.; Poulos, T.L. Ligand and Redox Partner Binding Generates a New Conformational State in Cytochrome P450cam (CYP101A1). *J. Am. Chem. Soc.* **2019**, *141*, 2678–2683. [CrossRef]
37. Poulos, T.L.; Follmer, A.H. Updating the Paradigm: Redox Partner Binding and Conformational Dynamics in Cytochromes P450. *Accounts Chem. Res.* **2022**, *55*, 373–380. [CrossRef]
38. Hollingsworth, S.A.; Batabyal, D.; Nguyen, B.D.; Poulos, T.L. Conformational selectivity in cytochrome P450 redox partner interactions. *Proc. Natl. Acad. Sci. USA* **2016**, *113*, 8723–8728. [CrossRef] [PubMed]
39. Pylypenko, O.; Schlichting, I. Structural aspects of ligand binding to and electron transfer in bacterial and fungal P450s. *Annu. Rev. Biochem.* **2004**, *73*, 991–1018. [CrossRef]
40. Hargrove, T.Y.; Lamb, D.C.; Smith, J.A.; Wawrzak, Z.; Kelly, S.L.; Lepesheva, G.I. Unravelling the role of transient redox partner complexes in P450 electron transfer mechanics. *Sci. Rep.* **2022**, *12*, 1–15. [CrossRef]
41. Tan, C.Y.; Hirakawa, H.; Suzuki, R.; Haga, T.; Iwata, F.; Nagamune, T. Immobilization of a Bacterial Cytochrome P450 Monooxygenase System on a Solid Support. *Angew. Chem.* **2016**, *128*, 15226–15230. [CrossRef]
42. Doğru, E.K.; Güralp, G.; Uyar, A.; Surmeli, N.B. Rational design of thermophilic CYP119 for progesterone hydroxylation by in silico mutagenesis and docking screening. *J. Mol. Graph. Model.* **2023**, *118*, 108323. [CrossRef] [PubMed]
43. Sakalli, T.; Surmeli, N.B. Functional characterization of a novel CYP119 variant to explore its biocatalytic potential. *Biotechnol. Appl. Biochem.* **2022**, *69*, 1741–1756. [CrossRef]

44. Sevrioukova, I.F.; Poulos, T.L.; Churbanova, I.Y. Crystal structure of the Putidaredoxin Reductase·Putidaredoxin electron transfer complex. *J. Biol. Chem.* **2010**, *285*, 13616–13620. [CrossRef] [PubMed]
45. Nguyen, K.; Nguyen, N.; Milhim, M.; Nguyen, V.; Lai, T.; Nguyen, H.; Le, T.; Phan, T.; Bernhardt, R. Characterization of a thermophilic cytochrome P450 of the CYP203A subfamily from Binh Chau hot spring in Vietnam. *FEBS Open Bio* **2021**, *11*, 124–132. [CrossRef] [PubMed]
46. Zhang, W.; Pochapsky, S.S.; Pochapsky, T.C.; Jain, N.U. Solution NMR Structure of Putidaredoxin–Cytochrome P450cam Complex via a Combined Residual Dipolar Coupling–Spin Labeling Approach Suggests a Role for Trp106 of Putidaredoxin in Complex Formation. *J. Mol. Biol.* **2008**, *384*, 349–363. [CrossRef] [PubMed]

**Disclaimer/Publisher's Note:** The statements, opinions and data contained in all publications are solely those of the individual author(s) and contributor(s) and not of MDPI and/or the editor(s). MDPI and/or the editor(s) disclaim responsibility for any injury to people or property resulting from any ideas, methods, instructions or products referred to in the content.